

pubs.acs.org/synthbio Research Article

Red Light-Activated Reversible Inhibition of Protein Functions by Assembled Trap

Peng Zhou,* Yongkang Jia, Tianyu Zhang, Abasi Abudukeremu, Xuan He, Xiaozhong Zhang, Chao Liu, Wei Li, Zengpeng Li, Ling Sun, Shouhong Guang, Zhongcheng Zhou, Zhiheng Yuan, Xiaohua Lu,* and Yang Yu*



Cite This: https://doi.org/10.1021/acssynbio.4c00585



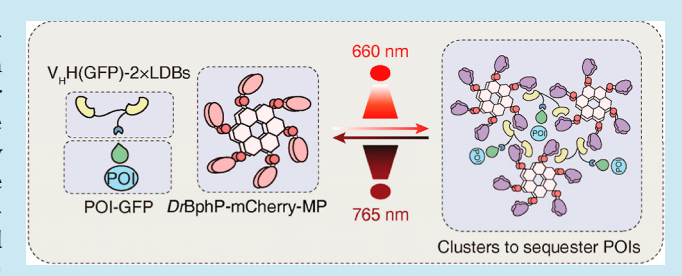
ACCESS

Metrics & More

Article Recommendations

s Supporting Information

ABSTRACT: Red light, characterized by superior tissue penetration and minimal phototoxicity, represents an ideal wavelength for optogenetic applications. However, the existing tools for reversible protein inhibition by red light remain limited. Here, we introduce R-LARIAT (red light-activated reversible inhibition by assembled trap), a novel optogenetic system enabling precise spatiotemporal control of protein function via 660 nm red-light-induced protein clustering. Our system harnesses the rapid and reversible binding of engineered light-dependent binders (LDBs) to the bacterial phytochrome *DrBphP*, which utilizes the



endogenous mammalian biliverdin chromophore for red light absorption. By fusing LDBs with single-domain antibodies targeting epitope-tagged proteins (e.g., GFP), R-LARIAT enables the rapid sequestration of diverse proteins into light-responsive clusters. This approach demonstrates high light sensitivity, clustering efficiency, and sustained stability. As a proof of concept, R-LARIAT-mediated sequestration of tubulin inhibits cell cycle progression in HeLa cells. This system expands the optogenetic toolbox for studying dynamic biological processes with high spatial and temporal resolution and holds the potential for applications in living tissues.

KEYWORDS: optogenetics, red light, DrBphP, nanobody, LARIAT, LDB

■ INTRODUCTION

Nature has evolved diverse organisms, including plants, algae, bacteria, fungi, and corals, which serve as rich sources of photoreceptors. 1,2 These photoreceptors usually absorb light from the 300 nm (ultraviolet; UV) to 800 nm (near-infrared light; NIR) range, triggering photochemical reactions that may induce conformational changes of photosensitive domains. Such light-induced conformational changes can be relayed to an attached effector domain to control various functions of proteins of interest (POIs) in optogenetics.^{3–5} Optogenetic technology has been widely used to modulate protein activity with high spatiotemporal resolution, such as CRY2-CIB1, iLID-sspB2, LOV2, 8,9 and the Magnet system. These photosensitive modules have been engineered into POIs or anchored to the plasma membrane to manipulate cellular functions, including cell dynamics,⁴ signal transduction,¹⁰ and gene expression.^{11,12} Additionally, optogenetic switches can also be applied to the split-protein reassembly system, allowing for light control of various bioactive proteins including nucleases, ^{13,14} recombinases, ^{15,16} proteases, ¹⁷ polymerases, antibodies, ¹⁹ and neurotoxins. ²⁰ However, most optogenetic strategies focus on protein activation; those strategies for the precise and effective inhibition of target proteins in a spatiotemporal-specific manner are very limited.

Traditional genetic perturbation methods, including gene mutation or deletion and RNA interference, have been widely used to study the protein function. Such strategies are typically irreversible and require a relatively long time to exert their effects and may cause various side effects. 21 For example, targeted deletion of many essential genes involved in embryonic development often results in embryonic lethality at early stages, which prevents further mechanistic investigation. 22,23 Optogenetic tools provide a promising opportunity for inhibiting the activities and functions of proteins with rapid reversibility and high spatiotemporal resolution. For example, the UV-B photoreceptor from Arabidopsis, UVR8, exists as homodimers in the dark and dissociates into monomers in response to UV-B light (280-310 nm).²⁴ Two copies of UVR8 fused with an endoplasmic reticulum (ER)processed protein were used to sequester the fusion protein in

Received: August 27, 2024 Revised: March 20, 2025 Accepted: April 22, 2025



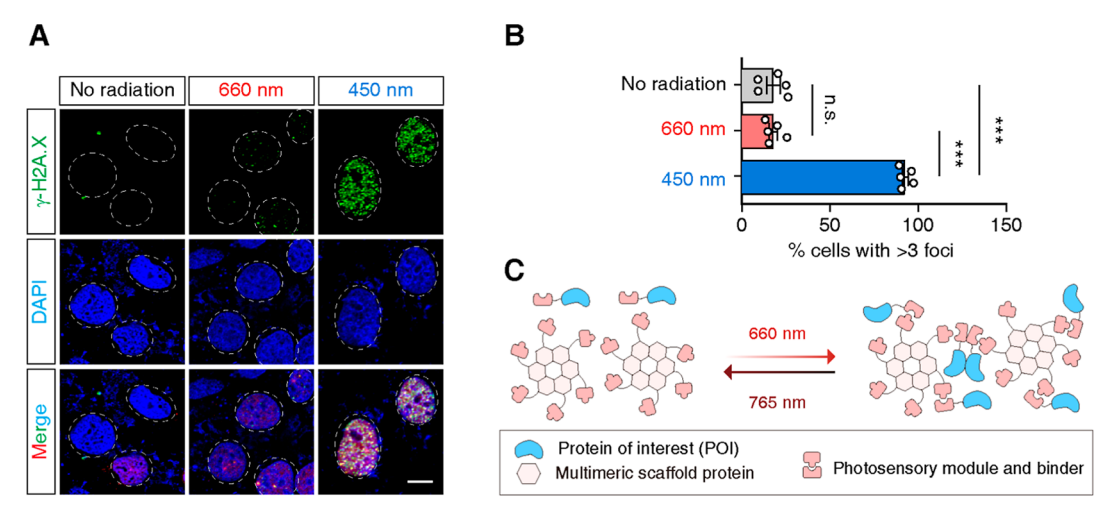


Figure 1. Prolonged exposure to blue light can cause DNA damage. (A) Fluorescence imaging of red light (660 nm) or blue light (450 nm)-induced γ -H2A.X expression (green) in U2OS cells. The dotted ovals indicate cell nuclei labeled by DAPI (blue). Scale bar: 10 μm. (B) Statistical data showing the percentage of γ -H2A.X foci positive cells among total DAPI-stained cells (n = 5 per group). The cells with more than three nuclear γ -H2A.X foci are regarded as γ -H2A.X positive cells. Data are presented as mean ± SEM. Statistical analysis was performed using one-way ANOVA with Tukey's multiple comparisons test. n.s., not significant; ***P < 0.001. (C) Schematic diagrams illustrating a hypothetical model of the red light-induced LARIAT system for sequestering POIs.

the ER in darkness.²⁵ UV-B light induced the release of the fusion protein from the ER by disassembly of the dimers. Another versatile optogenetic strategy called LARIAT (light-activated reversible inhibition by assembled trap) can also inhibit protein function by reversibly sequestering target proteins into large clusters in living mammalian cells.²¹

The LARIAT system based on blue light (450-500 nm) comprises a photoreceptor cryptochrome 2 (CRY2)-fused anti-GFP nanobody and a cryptochrome-interacting basichelix-loop-helix1 (CIB1)-fused multimeric protein (CIB1-MP). Upon blue light stimulation, the CRY2 proteins form simultaneously homo-oligomers and heterodimers with CIB1, which drives the formation of large clusters through interconnections among CIB1-MP to trap GFP-labeled proteins captured by anti-GFP nanobody. 26,27 However, the limited tissue penetration capability of blue light hampers LARIAT's in vivo application. Since the majority of optogenetic tools based on short-wavelength lights (below 600 nm) only have limited tissue penetration ability. 8,28,29 As an alternative, red and NIR light (650-900 nm) offer better tissue penetration and exhibit lower phototoxicity than other visible and UV light, 30,31 which make them a promising and ideal candidate for optogenetic tools.

Phytochromes are a class of bilin-binding photoreceptors found in plants, cyanobacteria or algae, bacteria, and fungi, that response to red and far-red light. 32,33 Phytochromes can typically switch between the red light-absorbing Pr state and the far-red light-responsive Pfr state.³⁴ Phytochrome B (PhyB), derived from Arabidopsis, uses the phytochromobilin chromophore to absorb red light (660 nm), further switching to an activated state, where it can bind to phytochrome-interacting factors (PIFs). This binding is reversible upon exposure to 720 nm NIR light. 5,35 The PhyB/PIFs system enables reversible nuclear localization of proteins, allowing for light-regulated control of protein positioning in mammalian cells and zebrafish.³⁶ The cyanobacterial phytochrome 1 (Cph1) uses phycocyanobilin as the chromophore and exhibits reversible dimer-to-monomer transition when light switches from 660 to 740 nm. ³⁷ Cph1 was fused to neurotrophin receptor TrkB and

FGFR1 to enable red light-inducible activation of receptor tyrosine kinases (RTK)-mediated signaling.³⁷ Although these red-light-activatable photoswitches have been developed and applied to regulate various biological activities, they require addition of exogenous chromophores in mammalian cells, thereby limiting their application.

The bacteriophytochrome photoreceptor 1 (BphP1) derived from Rhodopseudomonas palustris uses biliverdin (BV), a metabolite abundantly present in mammals, as the chromophore, ^{38,39} and can form a heterodimer with its natural binding partner RpsR2 upon 760 nm NIR light. The heterodimer dissociates in darkness or under 660 nm red light irradiation.³² However, PpsR2 can bind to the apoprotein of BphP1 irrespective of red light illumination, indicating high dark activity in the BphP1/PpsR2 system, 40,41 which greatly hinders its future utilization. Recently, several nanobodies were successfully selected to specifically bind to another BphP derived from Deinococcus radiodurans phytochrome (DrBphP) with low dark activity and high specificity under 654 nm red light illumination. 40-42 The DrBphP-nanobody heterodimers dissociate from the Pfr state to the fr state under 780 nm irradiation or in the darkness. Photoswitches based on DrBphP (i.e., NanoReD and MagRed) and its nanobody-based binders have been used to reversibly regulate gene expression and signal pathway in living cells and mammalian animals. 40,41 However, the red-light-controlled reversible inactivation system by trapping or sequestering POIs remains unavailable.

Here, we developed a versatile optogenetic strategy controlled by red light (660 nm) for reversibly inhibiting target proteins, by engineering the photosensor *Dr*BphP fused with MP and the nanobody-based binder light-dependent binders (LDBs) fused with the nanobodies of epitope tags, namely, R-LARIAT. R-LARIAT allows for rapid and reversible control of protein function by sequestering epitope-tagged proteins captured by the nanobodies of epitope tags into large clusters with red light illumination. We demonstrated that 2× LDBs connected by two copies of GGGGS-linker dramatically increased the clustering efficiency of GFP-tagged proteins. We also showed that R-LARIAT has been tested for disrupting

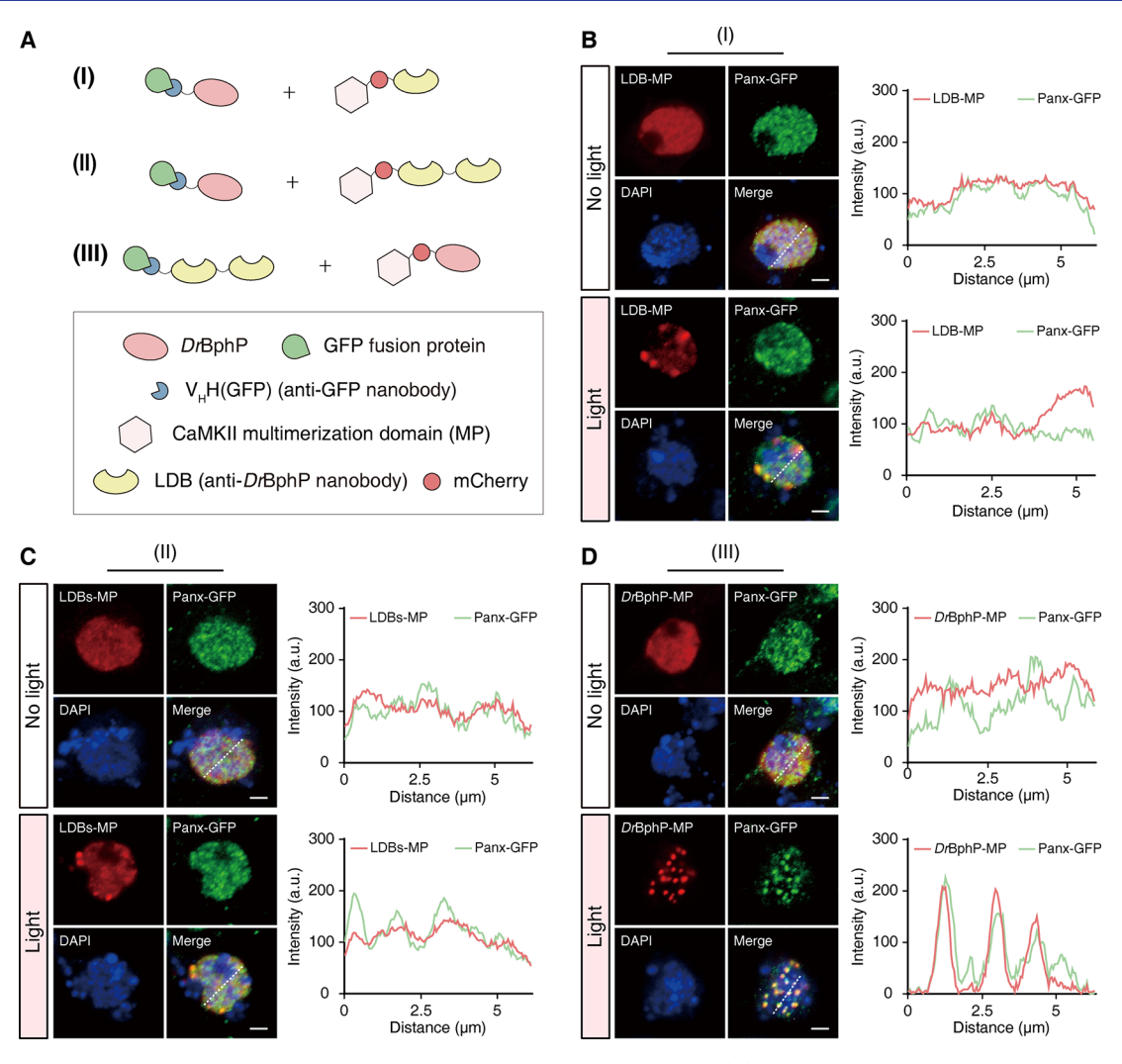


Figure 2. Design and validation of a novel protein clustering system induced by red light. (A) Schematic diagrams of three different scenarios for construction of fusion proteins. (B–D) Representative fluorescence images (left) and intensity profile (right) for Panx-GFP and LDB-MP (B), LDBs-MP (2× LDBs) (C), or DrBphP-MP (D) in Panx-GFP cells expressing the indicated constructs as A (I, II, or III) in Drosophila after 30 min of 660 nm illumination. The dotted lines in the merged images indicate the regions of interest for pixel intensity analysis. Scale bar: 2 μ m.

mitotic progression by trapping tubulin. Our R-LARIAT system takes advantage of red light with lower phototoxicity and deeper penetration ability and the photochemical properties of *DrB*phP, which uses the mammalian endogenous metabolite as its chromophore, offering new application prospects for living cells and organisms in the future.

RESULTS

Red Light Irradiation Did Not Cause Significant DNA Damage. The LARIAT is an effective strategy to inactivate POI by sequestering them into clusters with blue light irradiation. ^{21,26} However, long-term exposure to blue light might cause DNA damage to mammalian cells, which limits the application of this technology *in vivo*. ^{43,44} To evaluate whether red light is more advantageous in phototoxicity, we compared the effects of red light (660 nm) versus blue light (450 nm) using phosphorylated H2A.X (γ -H2A.X) staining as an indication of DNA damage in human U2OS cells (Figure 1A). After exposing the cells to either red or blue light for 2 hr, we observed a significantly increased percentage of γ -H2A.X positive nuclei under blue light exposure, but not red light (Figure 1B). The results indicate that red light may be a safer

choice for optogenetically manipulating the activity of target proteins over prolonged periods in living cells. Thus, considering that red light is capable of penetrating deeper tissues than shorter-wavelength blue light, ^{38,45} we hypothesized that a red light-dependent LARIAT system could be more suitable for *in vivo* applications (Figure 1C).

Creating a Red-Light-Induced Protein Clustering **System.** In the original LARIAT system, ^{21,26} the photosensitive protein CRY2 senses blue light, triggering its oligomerization and binding to CIB1, which subsequently forms clusters by self-assembly of MP (a CaMKII α multimerization domain) to trap GFP-tagged proteins (Figure S1). Therefore, we sought to replace CRY2 with a red lightresponsive protein. A truncated bacterial photoreceptor DrBphP, derived from D. radiodurans (hereafter named DrBphP for simplicity), was used, which maintains the minimal photoactive module (PAS-GAF-PHY; 60 kDa) required for sensing the red-light. Its photoswitching efficiency is close to that of the full-length DrBphP. 41,46,47 DrBphP offers several advantages for optogenetic control. First, DrBphP responds to a 660 nm-red light excitation wavelength, which causes almost no DNA damage to cells even after prolonged exposure

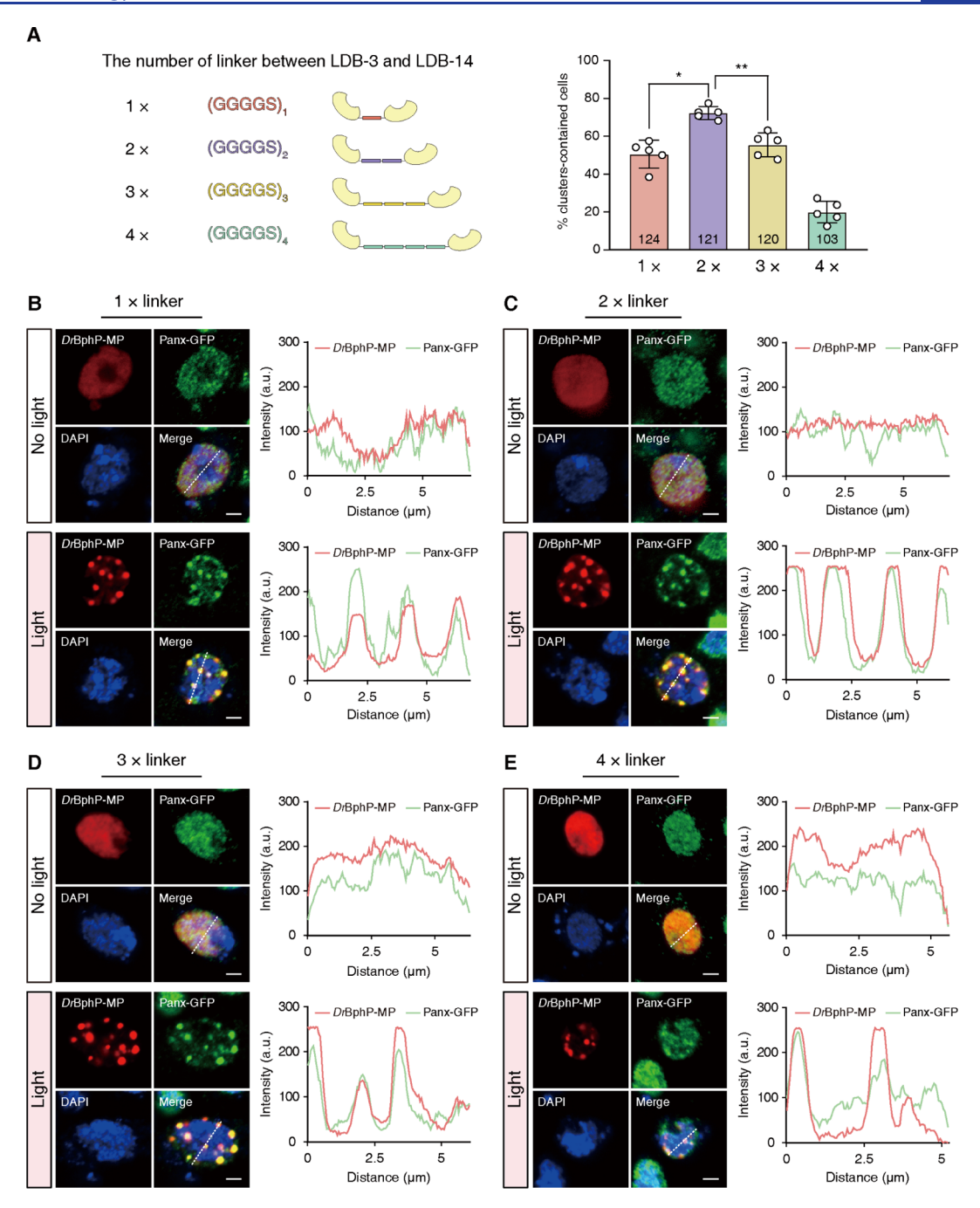


Figure 3. Optimization of the linker lengths in red-light-induced protein clustering system. (A) Left: The sequence and length of linkers between LDB-3 and LDB-14 for red-light-induced protein clustering system. Right: Statistical data of the percentage of cluster-containing cells among total mCherry positive cells after 30 min of 660 nm illumination (n = 5 per group). Data are presented as mean \pm SEM. Statistical analysis was performed using one-way ANOVA with Tukey's multiple comparisons test. *P < 0.05, **P < 0.01. (B–E) Representative fluorescence images (left) and intensity profile (right) for mCherry-MP and Panx-GFP in Panx-GFP cells transfected with the R-LARIAT plasmid containing the 1× linker (B), 2× linkers (C), 3× linkers (D), or 4× linkers (E) between LDB-3 and LDB-14 after 30 min of 660 nm illumination. The dotted lines in the merged images indicate the regions of interest used for pixel intensity analysis. Scale bar: 2 μ m.

(Figure 1A). Second, *Dr*BphP uses BV as a chromophore, a natural metabolite that exists in most eukaryotes. Third, nanobodies (i.e., LDB-3 and LDB-14) that specifically recognize and bind to the red light-activated form of *Dr*BphP are readily available.⁴¹

Therefore, we cloned the *Dr*BphP and *Dr*BphP-binding nanobodies (LDBs, light-induced dimerization binders) into a single expression vector separated by a virus-derived 2A linker to ensure relatively equal expression of both proteins. ^{48,49} We

designed and tested three distinct constructs, each corresponding to a specific combination of fusion proteins (Figures 2A and S2). In scenario (I), DrBphP was fused with the $V_HH(GFP)$ (anti-GFP nanobody) that binds specifically to GFP fusion proteins while one copy of LDB (LDB-3) was fused with a CaMKII α multimerization domain-mCherrry (MP-mCherry) (Figures 2A(I) and S2A), analogous to the blue light-dependent LARIAT (illustrated in Figure S1). Scenario (II) was similar to (I), except that $2\times$ LDBs (LDB-

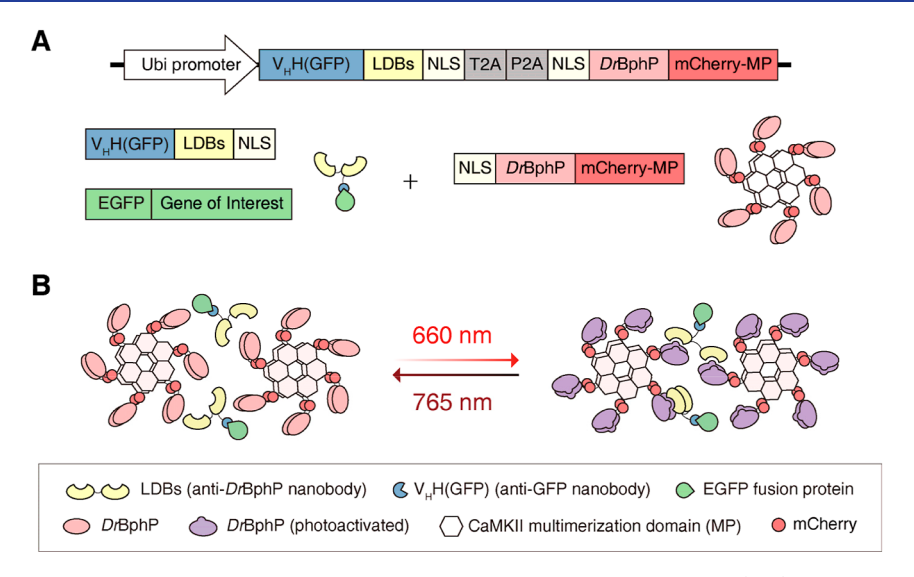


Figure 4. Red-light-induced protein clustering system for reversible sequestration of target proteins. (A,B) Schematic diagrams illustrating the modules (A) and working model (B) of the R-LARIAT system. The DrBphP-fused mCherry-MP undergoes a conformational change upon exposure to 660 nm red light and further binds to the LDBs-V_HH(GFP) fusion proteins to capture and sequester GFP-tagged proteins into large protein clusters.

3 and LDB-14) connected by a GGGGS linker were used [Figures 2A(II) and S2B]. In scenario (III), $2 \times LDBs$ were fused with the anti-GFP nanobody, while DrBphP was fused with the MP-mCherry [Figures 2A(III) and S2C].

To test the ability of these constructs to form clusters with GFP fusion proteins under red light illumination, we engineered a GFP knock-in tag to the C-terminus of the Panoramix (Panx) open reading frame (Panx-GFP) in ovarian somatic cells (OSCs) using CRISPR/Cas9 (Figure S3A-C). As a positive control, we tested the original blue lightdependent LARIAT system based on CRY2/CIBN (an Nterminal fragment of the CIB1) in Panx-GFP cells. Consistent with the published results, 21 the protein clustering capability depends on the wildtype CRY2 as well as the presence of both CIBN and blue light induction (Figure S4A-D). Then we tested the three constructs based on the DrBphP/LDBs using the same Panx-GFP cells with 660 nm red light illumination (Figure 2B-D). The construct (III) exhibited the most efficient clustering ability, with the mCherry spots (DrBphPmCherry-MP) almost completely coclustering with the GFP spots (Panx-GFP) in a red light-dependent manner (Figure 2D). In contrast, the other two constructs showed a significant amount of diffused GFP signals outside the mCherry spots (Figure 2B,C), indicating lower effectiveness in sequestering the GFP targets.

Optimization of the Red-Light-Induced Protein Clustering System. In scenario (III), efficient Panx-GFP clustering was observed when 2× LDBs (LDB-3 and LDB-14 connected by a GGGGS linker) were fused to the C-terminus of the anti-GFP nanobody [Figure 2A(III),D]. Moreover, the *DrB*phP exists as a head-to-head parallel dimer. S0,S1 We hypothesized that each LDB nanobody might bind to one component of the *DrB*phP dimer, respectively. Therefore, the distance between the two LDBs could be critical for their effective binding to the *DrB*phP dimer. First, we used a yeast two-hybrid (Y2H) assay to test whether the different GGGGS-linker lengths (1×, 2×, 3×, 4×) could affect the binding ability of 2× LDBs to *DrB*phP. Upon red light treatment, the yeast expressing *DrB*phP and 2× LDBs with different linker lengths

could grow on selective plates, and the interaction was strong enough to withstand 10 mM 3-AT (Figure S5A). On the other hand, only relatively weak interactions could be detected under dark conditions (Figure S5B), consistent with the fact that the interactions between DrBphP and $2\times$ LDBs induced by red light are much stronger.

Since no significant differences in the interactions between DrBphP and 2× LDBs with different linker lengths were seen by the Y2H assay, we directly tested the cluster-forming ability of these 2× LDBs utilizing R-LARIAT in Panx-GFP cells (Figure 3A, left panel). By counting the percentage of clustercontaining cells after 30 min of red-light illumination, we found that the constructs with two copies of the GGGGS-linker were the most efficient, in which about 70% of cells with R-LARIAT expression could form Panx-GFP clusters perfectly (Figure 3A, right panel and Figure 3B-D). The cluster formation efficiency for the other linker lengths was suboptimal (Figure 3B,D). Therefore, we developed a red-light-induced protein clustering system (R-LARIAT), which achieves optimal clustering efficiency when LDB-3 and LDB-14 are connected by two copies of the GGGGS-linker and fused with the anti-GFP nanobody, while DrBphP is fused with the MP-mCherry (Figure 4A,B).

Characterization of R-LARIAT. To fully characterize R-LARIAT, we first investigated the time-dependent protein clustering upon 660 nm red-light exposure. The protein clusters formed rapidly within the first few minutes, with approximately 50% of cells expressing R-LARIAT displaying detectable clusters after just 10 min of red-light stimulation (Figure 5A). This percentage reached nearly 100% after 80 min of 660 nm light exposure (Figure 5A). To further validate the sequestration efficiency of our R-LARIAT system, we used a commonly employed condensate-formation assay⁵² to quantify the percentage of GFP-tagged protein (GFP-Egg) trapped in the clusters. As target proteins were trapped in the condensates under red-light illumination, they could be precipitated by microcentrifugation, while free proteins escaping the clusters would remain in the supernatants.⁵³ Without light, the majority of GFP fusion targets was present

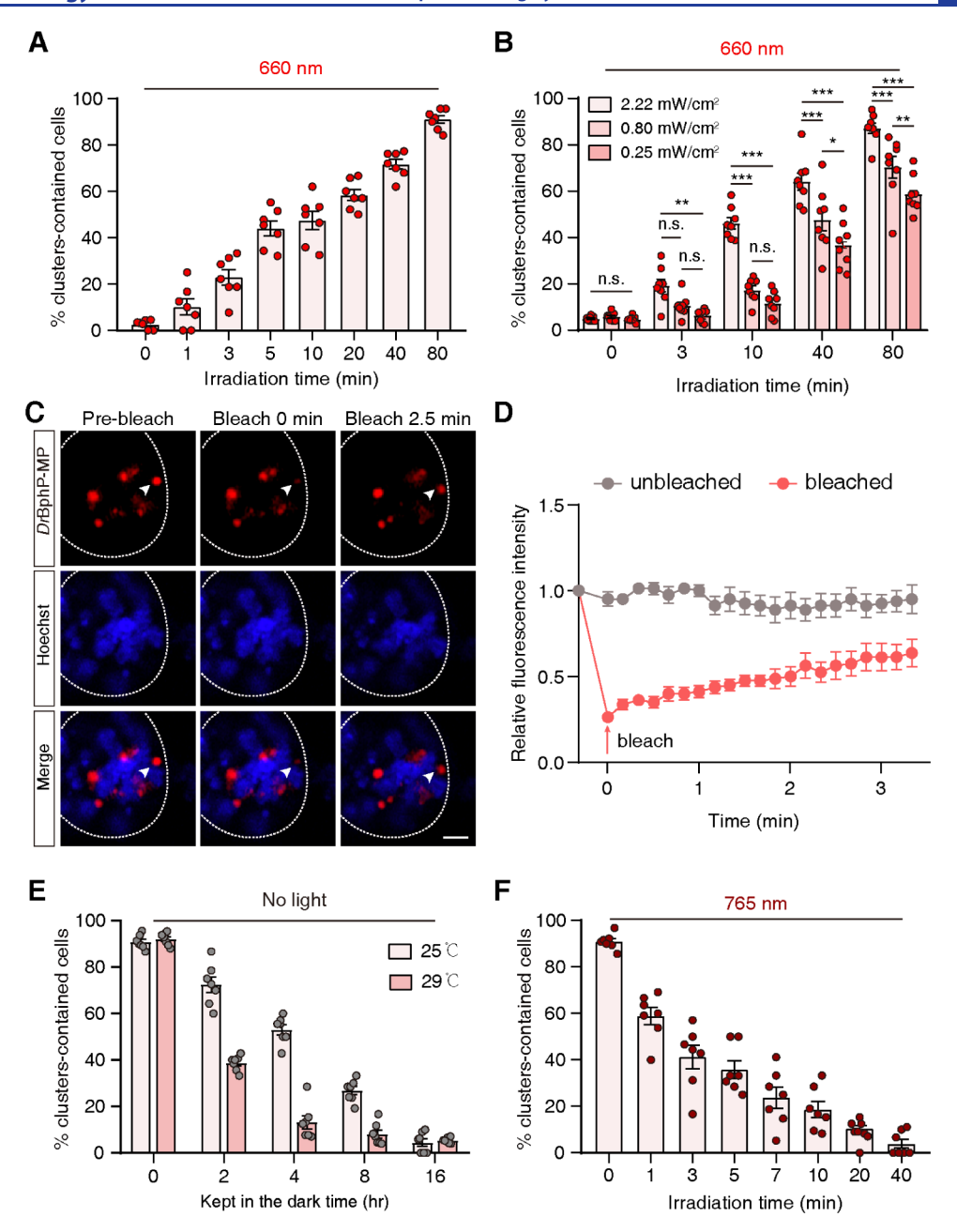


Figure 5. Characterization of R-LARIAT. (A) Statistical data of the percentage of cluster-containing cells induced by 660 nm of red light with different irradiation time. (B) Statistical analysis showing time-dependent cluster formation under 660 nm red light with varying intensities (2.22, 0.80, and 0.25 mW/cm²). The light intensities were calculated using the inverse square law based on the distances from the light source (10, 20, and 40 cm). Statistical analysis was performed using two-way ANOVA with Tukey's multiple comparisons test, n = 8 biological replicates per group. n.s., not significant P > 0.05; *P < 0.0

in the soluble fractions (supernatant) of the total cell lysates (Figure S6A,B). In contrast, upon 80 min of red light illumination, $\sim 90\%$ proteins were found in the pellets (Figure S6A,B), indicating that the majority of GFP fusion targets were sequestered into clusters.

Light intensity can modulate the activation efficiency of photosensitive modules, thereby regulating the efficiency of protein clustering.^{33,41} To investigate the light intensity-

dependent cluster formation, we varied the distance between the light source and the cells (10, 20, and 40 cm) to indirectly modulate the light intensity on cell surface (2.22, 0.80, and 0.25 mW/cm²), given that light intensity inversely correlates with the square of the distance from the source, as described by the inverse square law. ^{54–56} The results showed that even at a reduced light intensity of 0.25 mW/cm², approximately 60% of the cells still exhibited discernible protein clusters, indicating

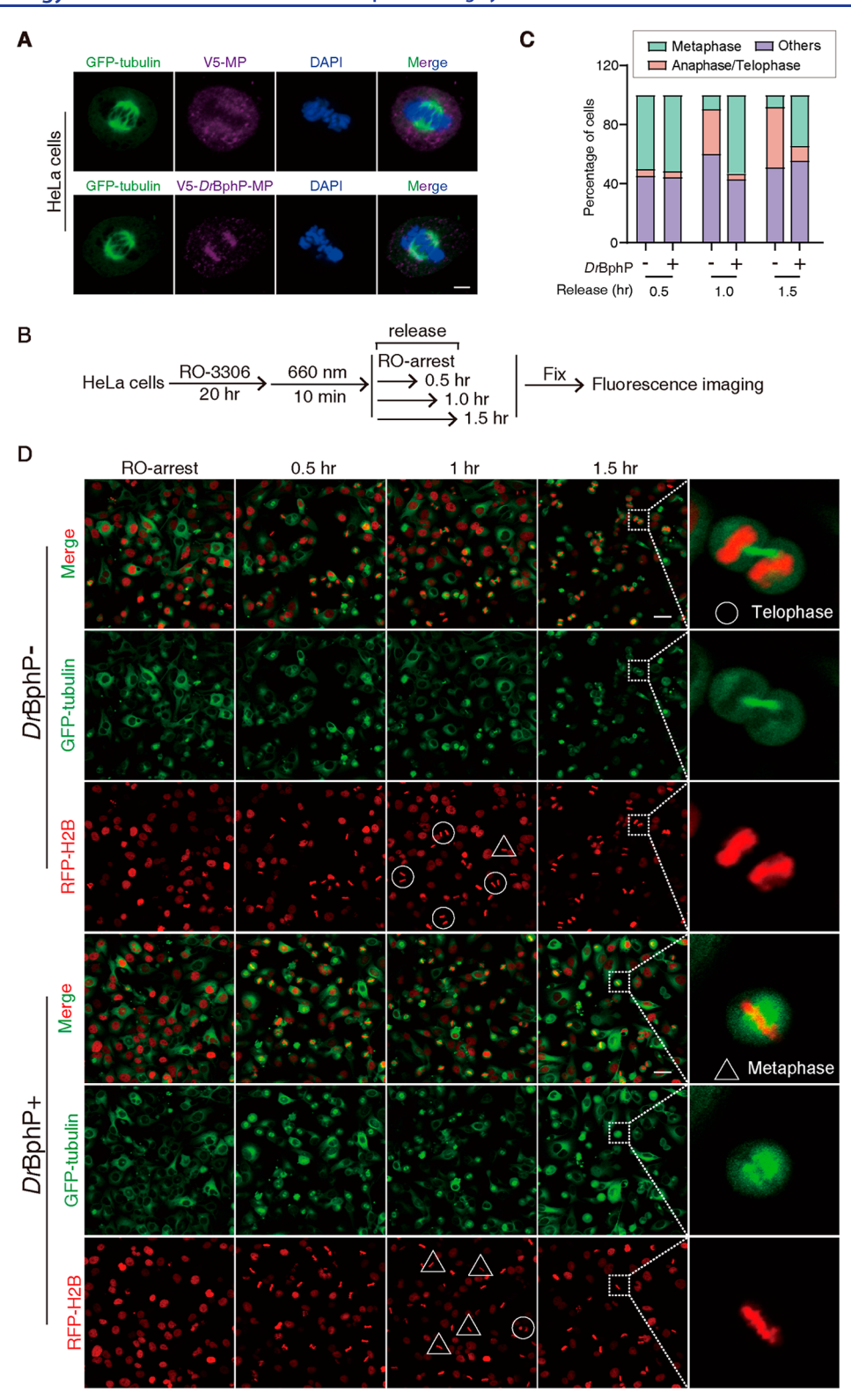


Figure 6. R-LARIAT can inhibit mitotic progression by trapping tubulin. (A) Representative fluorescence images showing the colocalization of GFP-tubulin and DrBphP-MP in HeLa cells expressing R-LARIAT upon red light illumination. Scale bar: 1 μ m. (B) Schematic depicting workflow of blockage of cell cycle. (C,D) Percentage of cells in different phases (C) and the expression of RFP-H2B and GFP-tubulin (D) after withdrawal of RO-3306 for 0.5, 1, and 1.5 hr in HeLa cells expressing R-LARIAT with (DrBphP+) or without DrBphP (DrBphP-) upon red light illumination. M phase cells were classified according to the morphologies of GFP-tubulin and chromosomes (RFP-H2B-labeled). White circles denote cells in telophase, while triangles denote cells in metaphase. Scale bar: 15 μ m.

that our system is responsive across a wide range of light intensities (Figure 5B). However, a significant reduction in clustering efficiency was seen with decreasing light intensity

under 40 and 80 min of red-light exposure (Figure 5B). These findings emphasize the importance of precise intensity control for optimal cluster formation.

To investigate the dynamic properties of protein clusters formed by R-LARIAT, we performed fluorescence recovery after photobleaching (FRAP) experiments in Panx-GFP cells expressing this system. After inducing cluster formation with 80 min of 660 nm light, we photobleached mCherry-tagged condensates and monitored fluorescence recovery over time (Figure 5C,D). Within minutes postphotobleaching, we observed substantial recovery of fluorescence within the clusters, indicating a rapid exchange of proteins between the condensates and the surrounding nucleoplasm (Figure 5C,D). This behavior resembles the dynamic exchange characteristic of liquid-liquid phase-separated droplets rather than static aggregates under current conditions. The reversibility of protein sequestration in R-LARIAT-mediated clusters likely prevents aggregation of trapped proteins, 57 suggesting that our system maintains physiological protein homeostasis while enabling precise optogenetic control.

Next, we examined the half-life of cluster dissociation following 80 min of red-light illumination. Initially, in darkness, the clusters dissociated slowly at room temperature (25 $^{\circ}\text{C})$ (Figure 5E). Since longer time are required to dissociate the clusters in Drosophila cells (cultured at 25 °C) compared to mammalian cells (cultured at 37 °C),^{21,26} we increased the culturing temperature of OSCs from 25 to 29 °C. The results showed that cluster dissociation could be accelerated ~2-3fold in darkness (Figure 5E). On the other hand, since the DrBphP/LDB system can be readily reversed by NIR light, 41,58 we also treated the aggregated R-LARIAT condensates with 765 nm NIR light. The results showed that clusters dissociated rapidly, with only half of the residual cells showing detectable clusters as early as 3 min after NIR illumination (Figure 5F). After 40 min of NIR light treatment, most of the clusters had disappeared. These results indicate that our R-LARIAT system can rapidly, reversibly, and effectively control the formation and dissociation of protein clusters in a light-dependent manner.

To better understand the dynamic characteristics of R-LARIAT condensates, we exposed the system to 660 nm red light for more prolonged periods (2, 8, and 24 hr), followed by assessment of cluster reversibility using 765 nm light (Figure S7A-C). Even after 24 hr of 660 nm light exposure, more than half of the cells exhibited cluster disassembly within 5 min of 765 nm light illumination (Figure S7C). However, a residual fraction (~20% of cells) maintained clusters even after 40 min of 765 nm light treatment (Figure S7C). These results suggest that while R-LARAIT condensates remain largely reversible even after prolonged 660 nm light exposure, a subset of clusters may undergo irreversible maturation. This observation aligns with previous studies demonstrating that optogenetic condensates can transition from dynamic liquid-like states to less dynamic gel-like or even solid-like states over time, potentially explaining the persistent clustering in a minority of cells despite extended dissociation attempts. 59-61

To further test the ability of R-LARIAT to sequester other proteins, researchers used either a GFP or RFP tag at their N-terminus. First, we engineered a GFP knock-in tag at the N-terminus of Eggless (Egg) open reading frame (GFP-Egg) in OSCs (Figure S8A). Similar to Panx-GFP, GFP-Egg could be completely sequestered by red light as the GFP-Egg spots almost completely coclustered with the MP-mCherry spots under red light illumination (Figure S8B). Next, we engineered the mCherry knock-in tag at the N-terminus of the Maelstrom (Mael) open reading frame (mCherry-Mael) in OSCs (Figure

S8C). In this case, an anti-mCherry nanobody was fused with the 2× LDBs instead of the anti-GFP nanobody. Similarly, efficient clustering was observed, with mCherry-Mael spots almost completely colocalizing with MP-GFP spots upon red light stimulation (Figure S8D). These results indicate that the R-LARIAT system can be used to effectively sequester a wide variety of proteins with different epitope tags at either N- or C-terminus.

R-LARIAT Successfully Sequesters Tubulin to Inhibit Mitosis. To demonstrate that our newly developed R-LARIAT could manipulate protein functions, we constructed a HeLa cell line stably expressing GFP-tubulin fusion. The DrBphP-MP fusion was expressed to sense the red light, and the V_H H(GFP)-LDBs fusion was used to capture the light-activated DrBphP aggregates in the GFP-tubulin cells. As a negative control, MP alone lacking the DrBphP module was used. Upon red light illumination, the DrBphP-MP signals (stained with the V5 tag antibody) colocalized with the GFP-tubulin signals (Figure 6A), indicating the successful sequestration of GFP-tubulin proteins into clusters. In contrast, MP alone remained diffusely distributed with little or no colocalization with GFP-tubulin (Figure 6A).

To examine functional consequences of the GFP-tubulin sequestration, we synchronized the HeLa cells using a CDK1 inhibitor (RO-3306), which arrested most of cells at the G2/M transition. 62 The cells were then illuminated with 660 nm red light for 10 min to facilitate GFP-tubulin sequestration. Subsequently, RO-3306 was washed away to allow the cell cycle to proceed. Cells were collected at various time points after RO-3306 release (0.5, 1, and 1.5 hr) to assess their cell cycle stages (Figure 6B). Based on GFP-tubulin and chromatin morphologies (labeled with RFP-H2B),⁶³ M phase cells could be classified into three categories: metaphase (highlighted with triangles); anaphase/telophase (highlighted with circles); and others. Consistent with the published results, 21 sequestering GFP-tubulin by R-LARIAT led to a significantly increase in the percentage of metaphase cells, accompanied by a decrease in the anaphase/telophase phase cells at 1 and 1.5 hr after RO-3306 withdrawal (Figure 6C,D). This phenomenon was not observed in the control cells lacking the DrBphP module (Figure 6C,D). These results suggest that R-LARIAT effectively slows cell cycle progression by trapping GFPtubulin. Therefore, R-LARIAT can be used to efficiently manipulate protein functions in living cells with a high spatiotemporal resolution.

DISCUSSION

In this study, we introduce R-LARIAT, a novel optogenetic system designed for precise, reversible control of protein function through 660 nm red-light-induced clustering. The system utilizes a MP scaffold fused with the photosensitive bacterial phytochrome DrBphP, alongside DrBphP-specific nanobodies (2× LDB) conjugated to single-domain antibodies targeting specific epitope-tagged proteins. Upon exposure to 660 nm red light, DrBphP undergoes a conformational change that enables binding to the LDBs-V_HH(GFP) fusions. This interaction subsequently captures and sequesters GFP fusion target proteins in large protein clusters formed via MP multimerization (Figure 4). A key innovation of R-LARIAT lies in its utilization of red light, which offers several practical and biological advantages. The red light-responsive photosensitive module (DrBphP) leverages endogenous BV as its chromophore, eliminating the need for exogenous chemicals

and reducing potential experimental artifacts. This feature, combined with the red light's inherent properties of lower phototoxicity and superior tissue penetration, makes R-LARIAT particularly suitable for studying protein function in living organisms over extended periods and at greater tissue depths.

Using R-LARIAT, we successfully obstructed the mitotic process by sequestering tubulin in HeLa cells, indicating that our newly developed R-LARIAT can effectively manipulate protein function in living cells. The cells were exposed to red light for just 10 min, which was sufficient to slow down the cell cycle, indicating relatively high light sensitivity of our system. Nevertheless, many applications may require blocking protein function for a longer time (hours to days) to observe an effect. For instance, in a light-inducible nuclear export system, cells were illuminated for 24 hr with 460 nm blue light.⁶⁴ In our study, a 2 hr exposure to blue light significantly increased γ -H2A.X staining signals in U2OS cells, indicative of DNA damage (Figure 1A). In another study, the SEAP production as an indicator revealed that 1 hr blue light exposure resulted in marked cytotoxicity, and cell viability was significantly decreased in HEK293 cells.³³ Collectively, exposure to blue light as short as 1 hr may cause measurable cytotoxicity in mammalian cells. Consequently, engineering red-light-based optogenetic tools can effectively minimize cellular damage, particularly in scenarios that require prolonged exposure.

To optimize the R-LARIAT system, we designed and tested three different combinations of fusion proteins (Figure 2A). In scenarios (I) and (II), the DrBphP was fused with the anti-GFP nanobody, while the multimeric protein (MP-mCherry) was fused with either one (I) or two (II) copies of LDB nanobody that can bind to the light-induced form of DrBphP. Although we observed some promising aggregation upon lightillumination (Figure 2B,C), there were still significant fractions of free GFP proteins that escaped clustering. We reasoned that either the MP-mCherry module interfered with the capturing function of LDB or preattachment of DrBphP to the target protein somehow restricted its light-sensing function as DrBphP usually exists as a head-to-head parallel dimer. 50,51 Therefore, we swapped the fusion protein partners by linking DrBphP with MP-mCherry while connecting the LDB with the anti-GFP nanobody (Figure 2A, scenario III). In this case, the red spots that indicated the DrBphP-mCherry-MP fusions almost completely overlapped with the GFP spots (Panx-GFP fusion targets) upon red-light illumination, indicating a near complete association of the GFP targets by R-LARIAT (Figure 2D, Light). Moreover, the diffused GFP signals seen in the no light condition were largely absent in scenario III when treated with light (Figure 2D), a phenomenon not observed with the other two combinations (Figure 2B,C). These results indicate that different module combinations may contribute to the functionality of the optogenetic system.

In addition, a suitable linker length may be crucial for engineering artificial protein binders. In general, shorter linkers can minimize unnecessary spacing for efficient interactions while longer linkers can reduce potential steric hindrance between functional domains and provide significant flexibility for large constructs. However, excessive flexibility may result in nonspecific interactions with other molecules, potentially compromising the structural integrity or folding of the fusion proteins. Since *DrBphP* exists as a head-to-head parallel dimer, a series of GGGGS linkers with different copies (1 to 4×) separating LDB-3 and LDB-14 were tested. We found that

two copies of the GGGGS-linker were the most effective for cluster formation (Figure 3). Therefore, optimizing linker length to balance the flexibility and stability of fusion proteins may be preferable for designing artificial protein binders.

The R-LARIAT demonstrates high light sensitivity and stability. Red-light-induced cluster formation could be readily observed within the first few minutes, with about 50% of cells displaying detectable clusters after just 10 min of red-light illumination. The percentage of cells with the aggregated clusters would increase to nearly 100% after 80 min of illumination. This rapid and efficient clustering underscores the system's potential for time-sensitive experimental applications. However, some residual protein activity might persist, potentially causing unintended effects, which might limit its application in situations requiring complete inhibition of the protein function.⁶⁷ Cluster dissociation in R-LARIAT exhibits distinct kinetics depending on the environmental conditions. In darkness, clusters disassemble gradually at room temperature, with about 20% of cells losing clusters after 2 hr of redlight withdrawal. The slower dissociation rate in darkness is likely due to the low reversion rate of the photoreceptor. Previous studies have shown that DrBphP exhibits biexponential slow dark reversion from the photoactivated Pfr state back to ground Pr state, with about 30% reversion rate for 2 hr of darkness, which is much slower than that of another phytochrome, *RpB*phP1. 40,41,47,68 Moreover, the dark reversion of DrBphP can be hindered by the nanobody binding and dimerization. 41,68 In contrast, exposure to 765 nm NIR light triggers rapid cluster dissociation, with ~50% of clustercontaining cells exhibiting reversal within 3 min of light exposure (Figure 5F). This accelerated disassembly is consistent with the previously documented rapid photoconversion of DrBphP to the Pr state under NIR light illumination. 41,47 The dual dissociation characteristics of R-LARIAT present distinct experimental advantages. The slow dark reversion enables sustained protein inhibition even after light withdrawal, which is beneficial for studies requiring prolonged functional blockade. Conversely, the rapid NIRinduced disassembly facilitates precise temporal control, making R-LARIAT suitable for applications demanding quick reversibility. This flexibility positions R-LARIAT as a versatile tool for diverse optogenetic research paradigms.

In our system, the use of single-domain antibodies (nanobodies) to capture epitope-tagged proteins allowed us to extend the method to multiple proteins. To validate the broader applicability of our system, we also tested other tags (i.e., mCherry) and observed a similar clustering capability, comparable to the GFP-tagged system. Therefore, our R-LARIAT system holds considerable potential for manipulating a variety of proteins with various epitope tags. Nanobodies with advantageous features, such as small size (\sim 15 kDa), stability and excellent tissue penetration, ⁶⁹ provide an excellent tool for genetic engineering in living cells. In contrast, the larger size of the conventional antibodies, which consist of heavy and light chains connected by disulfide bonds, restrict their applications in cells. 70 Nevertheless, certain nanobodies selected in vitro may face some issues when used in cellular environments. Testing the ability of nanobodies to bind their targets in a cell-based assay such as yeast two-hybrid (Y2H) may be helpful in resolving the issues.

In this study, we developed a versatile optogenetic method, R-LARIAT, to inhibit target protein functions. Our R-LARIAT system holds the potential to be applied in live transparent

ı

animals such as Caenorhabditis elegans or Zebrafish due to lower phototoxicity and better tissue penetration ability of 660 nm red light. Moreover, our R-LARIAT system should be useful for controlling many cellular processes by trapping diverse target proteins into clusters to sequester their functions. Our R-LARIAT system is especially useful for manipulating proteins whose biological functions depend on proper localization (e.g., tubulin). Similar examples include proteins that must function specifically in the nucleus or cytoplasm. For instance, one could envision sequestering a nuclear protein in the cytoplasm, similar to the trap-away system used in yeast.⁷¹ From a biological perspective, the R-LARIAT system could be valuable for sequestering maternal proteins deposited in fertilized embryos, thereby aiding in the dissection of their roles in oocytes versus early embryos. Alternatively, the R-LARIAT may be coupled with the E3/ ubiquitin/proteasome pathway to simultaneously sequester and degrade target proteins, further increasing the robustness of this optogenetic tool. In conclusion, our newly developed R-LARIAT provides researchers with powerful and flexible tools for modulating protein activity with high spatiotemporal resolution and reversibility.

MATERIALS AND METHODS

Plasmid Construction. The core modules of R-LARIAT, a truncated version DrBphP without the histidine kinase domain, and the nanobody-based binders for DrBphP, LDB-3/LDB-14, were amplified from the NanoReD system⁴¹ and then were cloned into the pENTR4 vector (Thermo Fisher Scientific, A10465). Subsequently, they were recombined into the pUbiquitin gateway vector for expression in flies and the pCAGG gateway vector for expression in mammals through LR Clonase II (Invitrogen)-mediated recombination. The sequence of CIBN (an N-terminal fragment of the CIB1) and CRY2PHR (the photolyase homology region of CRY2) or CRY2PHR (D387A) (a mutant of CRY2) in blue lightmediated LARIAT system was amplified from those vectors in published paper.²⁷ The anti-GFP nanobody [V_HH(GFP)] and anti-mCherry nanobody sequences were cloned from a PHR-V_HH(GFP) vector²⁷ and a pGEX6P1-mCherry-Nanobody vector (Addgene, 70696), respectively. All primers used in this study are listed in Supporting Information Table 1.

The gRNAs targeting Panoramix (Panx), Maelstrom (Mael), and Eggless (Egg) of Drosophila were designed using the Web site: http://crispor.tefor.net/ and then were cloned into the CFD4 vector (Addgene, 49411), following previously described methods.⁷² The sequence of gRNAs utilized in this research is listed in Supporting Information Table 2. Gene fragments of tubulin and H2B were amplified from the cDNA of HEK293T cells using PCR and then were cloned into the pENTR4 vector. Subsequently, pENTR4-tubulin was recombined into the MSCV-GFP-Gateway vector through the LR reaction, and pENTR4-H2B was recombined into the pCW-λN-2 × flag-RFP-Gateway. The plasmids information and genes sequence utilized in this research are listed in Supporting Information Tables 3 and 4.

Cell Culture and Generation of Stable Cell Lines. The OSCs from *Drosophila*, HeLa cell line, and U2OS cells used in this study originated from the Cold Spring Harbor Laboratory in the United States. The OSC cells were typically cultured in the Shields and Sang M3 Insect Media (Sigma) supplemented with 10% FBS (Fetal Bovine Serum), 5% fly extract, 0.6 mg/mL glutathione, and 10 mg/mL insulin in a constant

temperature (25 $^{\circ}$ C) and humidity incubator. The HeLa cells and U2OS cells were generally cultured in a DMEM medium supplemented with 10% FBS and 1% penicillin/streptomycin in a constant temperature (37 $^{\circ}$ C) and humidity (60%) incubator with 5% CO₂.

Cells were seeded in 6-well plates to reach approximately 80% confluency for transfection. The Panx-GFP, GFP-Egg, and mCherry-Mael cell lines were established using CRISPR/ Cas9.⁷³ The OSC cells were cotransfected with the CFD4 plasmids expressing sgRNA targeted Panx, Egg or Mael (1.5 $\mu g/\text{well}$), the homologous arm (1.5 $\mu g/\text{well}$) containing selective markers and inserted tags (GFP or mCherry), and the plasmid encoding wild-type spCas9 (1.5 μ g/well) using FuGENE HD (Promega, E2312). The stable cell lines were generated by antibiotic selection according to the relative resistance genes at 48 h post-transfection. The Panx-GFP and GFP-Egg cell line were selected by blasticidin (10 μ g/mL), while the mCherry-Mael cell line was selected by hygromycin (50 μ g/mL) in OSCs. HeLa cells were cotransfected with the MSCV-GFP-tubulin plasmid (2 μ g/well) and the pCW- λ n-2 × flag-RFP-H2B plasmid (2 µg/well) using Lipofectamine 2000 (Invitrogen, 11668030). The stable GFP-tubulin/RFP-H2B cell line was selected by puromycin (1 μ g/mL) and neomycin (400 μ g/mL) in HeLa cells. Then the GFP-tubulin/RFP-H2B cell line was transfected with the R-LARIAT plasmids by using Lipofectamine 2000 and selected by blasticidin (10 μ g/mL) for the establishment of the GFP-tubulin/RFP-H2B/R-LARIAT cell line. All of the cell lines were validated via genomic PCR, RT-PCR, and Western blotting.

Photoexcitation Experiment. Panx-GFP cells were transfected with LARIAT plasmids by using FuGENE HD. Next, the cells expressing LARIAT constructs were dissociated and seeded on the glass coverslip in a 6-well plate (Corning) at 48 h post-transfection and allowed to adhere for at least 6 h before imaging. To avoid premature exposure to unintended light sources, cells were shielded with aluminum foil and kept in a darkroom under proper cultural conditions before irradiation and imaging. In the construction of the R-LARIAT assay, cells were exposed to 660 nm red light (20 mW/cm²) for a series of time, then fixed with 4% formaldehyde, and subjected to imaging using a laser confocal microscope (ZIESS-LSM700). In the cluster disassembly assay, cells were first exposed to 660 nm red light (20 mW/cm²) for 80 min to form protein clusters. Next, the cells were kept in darkness or exposed to 765 nm NIR light for different periods of time and then used for imaging or dissociation for Western blot. In the blue-light-based LARIAT assay, cells expressing LARIAT plasmids were illuminated with 450 nm blue light (20 mW/ cm²) for 10 min prior to imaging.

To mitigate the phototoxicity and photobleaching, our illumination system employed a multipoint light source configuration that uniformly covers the entire sample area, ensuring highly consistent light exposure and thereby enabling precise optogenetic induction. To prevent unintended activation of light-sensitive proteins, all experimental operations up to this point were performed under safe green or orange light conditions. All LED lights (20 mW/cm²) were purchased from Xuzhou Ai Jia Electronic Technology Co., Ltd. (Xuzhou, China).

Fluorescence Recovery after Photobleaching. Panx-GFP cells expressing R-LARIAT were exposed to 660 nm of red light (20 mW/cm²) for 80 min to drive protein cluster formation. Then FRAP was performed using a Zeiss LSM 980

confocal microscopy with a 594 nm laser. The fluorescent spots were bleached with 20% laser power and a 0.9 s dwell time for one pulse, and images were acquired every 10 s for 3.5 min. Fluorescence intensity at the bleached locus and a distal unbleached control spot was measured at each time point using ImageJ (Fiji edition, NIH). The real-time fluorescence intensities were normalized to the prebleached values of the spots.

Y2H Assay. The Y2H assays were performed using the Y187 strain. The fragments of *Dr*BphP were cloned into the pGBKT7 DNA-BD vector (Takara, Cat. #630443), while LDB-3 and LDB-14 fragments connected by 1× linker, 2× linkers, 3× linkers, or 4× linkers were cloned into the pGADT7 AD vector (Takara, Cat. #630442). The colonies containing double plasmids were selected on -Leu-Trp YSD plates and confirmed by colony PCR. To detect the protein—protein interactions under red light illumination, single colonies in serial dilutions were plated onto -Leu-Trp-His plates with varying concentrations of 3-AT. The empty BD vectors without *Dr*BphP were used as a negative control.

Western Blot. The cells were digested by trypsin and collected into a centrifuge tube and then were washed twice with PBS and lysed in RIPA buffer (50 mM Tris-HCl, pH 8.0, 150 mM NaCl, 1% NP-40, 1% sodium deoxycholate, 0.1% SDS, 0.1 mM DTT, PMSF and protease inhibitor cocktail). The lysates were clarified by centrifugation at 15,000g for 15 min, and the supernatants were subjected to boil at 95 °C for 5 min with Laemmli sample buffer. Then proteins were transferred to PVDF membranes after SDS-PAGE electrophoresis for immunoblotting. The antibodies used in this study include rabbit anti-EGFP (ZENBIO, 300943), mouse anti-Flag (Sigma, clone M2, F3165), mouse antitubulin (Invitrogen, MA5-31466), and HRP-conjugated secondary antibodies (antirabbit, Invitrogen 31460; antimouse, Invitrogen 31430). Signals were acquired using an automatic chemiluminescence imaging system (Tanon 5200) and analyzed by ImageJ (Fiji edition, NIH).

Cell Cycle Synchronization and Photoexcitation. The Cdk1 inhibitor RO-3306 was used to enable cycle synchronization of HeLa cells expressing GFP-tubulin and RFP-H2B at the M phase, as described previously. 74,75 The GFP-tubulin/ RFP-H2B/R-LARIAT cells were prearrested at the G2/M border by treatment with 6 μ M RO-3306 (Selleck, S7747) for 20 hr. To determine the effect of trapped tubulin on the cell cycle, these cells were exposed to 660 nm red light (20 mW/ cm²) for 10 min and then were washed with prewarmed PBS (37 °C) containing Ca²⁺ and Mg²⁺ (PBS+) to prevent detachment of cells. After being incubated in prewarmed medium for 0, 1, or 1.5 hr, cells were fixed with 4% formaldehyde at room temperature for 20 min. Imaging of cells was performed using a Zeiss LSM700 to distinguish mitotic subphases. The percentage of cells in each category among the M phase was calculated according to their morphological characteristics.

Immunofluorescence and Imaging. The cells were digested and seeded on a sterilized coverslip (22×22 mm) in a six-well plate at 60% confluency to allow cells to settle and adhere onto the coverslip. Then culture medium was removed, and the cells were washed twice with PBS and fixed with 4% paraformaldehyde at room temperature for 15–20 min prior to immunostaining. Then the cells were incubated with 0.5% PBST (PBS containing 0.1% Triton X-100) at room temperature for 20 min and were blocked with blocking buffer

(0.1% PBST containing 1% BSA) at room temperature for 1 hr. Then the cells were incubated with the primary antibody against EGFP (ZENBIO, 300943), mCherry (Abcam, ab125096), γ -H2A.X (CST, 9718S) or V5 (Abclone, AE089) diluted in primary antibody dilution buffer (Abclone, P0103) at room temperature for 1 hr. The cells were then incubated with the secondary antibody at room temperature in the dark for 1 hr. The secondary antibodies used in this study include goat antirabbit-Alexa Fluor 488 (Beyotime, A0423), goat antimouse-ABflo 555 (ABclonal, AS057), and goat antirabbit-ABflo 647 (ABclonal, AS060). Images were captured using laser scanning confocal microscopy (ZIESS-LSM700) and processed with ImageJ (Fiji edition, NIH).

Light Intensity Calculation. In this study, a uniform LED surface light source with a radius (d_0) of 5 cm was used. The initial light intensity at the LED surface (I_0) was measured at a density of 20 mW/cm². The LED was positioned horizontally, emitting light downward in a diffuse manner, approximating an expanding uniform plane wavefront. Given that the LED functions as a uniformly radiating planar source, the spatial decay of irradiance can be approximated by the inverse-square law. The light intensity (I_d) at a given distance (d) from the LED's center was calculated using the formula: $I_{(d)} = I_0 \times (d_0^2/d^2)$. The actual distance (d) is defined as the sum of the distance from the LED surface and the radius of the LED source (d_0) . Based on this calculation, the light intensities at distances of 10, 20, and 40 cm from the LED surface were approximately 2.22, 0.80, and 0.25 mW/cm², respectively.

ASSOCIATED CONTENT

Supporting Information

The Supporting Information is available free of charge at https://pubs.acs.org/doi/10.1021/acssynbio.4c00585.

Schematic representation of blue-light-induced optogenetic clustering system by LARIAT, schematic diagrams of three different constructs for protein clustering system induced by red light, construction of the Panx-GFP cell line, design and validation of LARIAT modules for blue-light-induced cluster formation, interactions between DrBphP and 2× LDBs, quantitative analysis of sequestration efficiency across GFP-Egg, time-dependent on cluster dissociation after prolonged periods of red-light exposure, red-light-induced cluster formation in GFP-Egg and mCherry-Mael cells, primers used in this study, gRNA sequences for knock-in in OSCs, plasmids information used in this study, and the gene sequence of LARIAT and R-LARIAT modules (PDF)

AUTHOR INFORMATION

Corresponding Authors

Peng Zhou — Division of Life Sciences and Medicine, University of Science and Technology of China, Hefei 230027, China; Guangzhou Women and Children's Medical Center, Guangzhou Medical University, Guangzhou 510623, China; Institute of Biophysics, Chinese Academy of Sciences, Beijing 100101, China; orcid.org/0009-0008-1625-3586; Email: zhoupe@mail.ustc.edu.cn

Xiaohua Lu — Institute of Biophysics, Chinese Academy of Sciences, Beijing 100101, China; Email: luxiaohua@ibp.ac.cn

Yang Yu — Guangzhou Women and Children's Medical Center, Guangzhou Medical University, Guangzhou 510623,

China; Institute of Biophysics, Chinese Academy of Sciences, Beijing 100101, China; Email: yuyang@gwcmc.org

Authors

- Yongkang Jia School of Life and Health Sciences, Hubei University of Technology, Wuhan 430068, China
- Tianyu Zhang Guangzhou Women and Children's Medical Center, Guangzhou Medical University, Guangzhou 510623, China; Institute of Biophysics, Chinese Academy of Sciences, Beijing 100101, China
- Abasi Abudukeremu Guangzhou Women and Children's Medical Center, Guangzhou Medical University, Guangzhou 510623, China; Institute of Biophysics, Chinese Academy of Sciences, Beijing 100101, China
- Xuan He Guangzhou Women and Children's Medical Center, Guangzhou Medical University, Guangzhou 510623, China
- Xiaozhong Zhang Guangzhou Women and Children's Medical Center, Guangzhou Medical University, Guangzhou 510623, China
- Chao Liu Guangzhou Women and Children's Medical Center, Guangzhou Medical University, Guangzhou 510623, China
- Wei Li Guangzhou Women and Children's Medical Center, Guangzhou Medical University, Guangzhou 510623, China
- Zengpeng Li Key Laboratory of Marine Genetic Resources, State Key Laboratory Breeding Base of Marine Genetic Resources, Fujian Key Laboratory of Marine Genetic Resources, Fujian Collaborative Innovation Centre for Exploitation and Utilization of Marine Biological Resources, Third Institute of Oceanography Ministry of Natural Resources, Xiamen 361005, China
- Ling Sun Center for Reproductive Medicine, Guangzhou Women and Children's Medical Center, Guangzhou Medical University, Guangzhou 510623, China
- Shouhong Guang Division of Life Sciences and Medicine, University of Science and Technology of China, Hefei 230027, China
- Zhongcheng Zhou Guangzhou Women and Children's Medical Center, Guangzhou Medical University, Guangzhou 510623, China
- Zhiheng Yuan Guangzhou Women and Children's Medical Center, Guangzhou Medical University, Guangzhou 510623, China; Institute of Biophysics, Chinese Academy of Sciences, Beijing 100101, China

Complete contact information is available at: https://pubs.acs.org/10.1021/acssynbio.4c00585

Author Contributions

Y.Y., X.L., and P.Z. designed this study. P.Z. carried out the experiments and analyzed the data. Y.J., T.Z., A.A., X.H., and X.Z assisted in experiments. C.L., W.L., Z.L, and L.S contributed materials. P.Z., S.G., Z.Z., Z.Y., X.L, and Y.Y. discussed the results and drafted the manuscript. All authors have read and approved the final manuscript.

Notes

The authors declare no competing financial interest.

ACKNOWLEDGMENTS

We would like to thank the Xiaobo Wang Laboratory for generously providing the original blue light-mediated LARIAT plasmids as gifts. We also thank Xing Jia and Qing Bian from Center for Biological Imaging (CBI), Institute of Biophysics, Chinese Academy of Sciences, for technical support with LSM980 Confocal-Plus imaging and image analysis. We extend our sincere gratitude to Dr. Changmao Chen for helpful discussions and comments on this work. This work was supported in part by grants from the Ministry of Science and Technology of China (2019YFA0508903 and 2017YFA0504200 to Y.Y.) and the National Natural Science Foundation of China (81921003 and 32170605 to Y.Y.). Y.Y. was additionally supported by the start-up fund from Guangzhou Women and Children's Medical Center.

ABBREVIATIONS

LARIAT, light-activated reversible inhibition by assembled trap; UV, ultraviolet; NIR, near-infrared light; POIs, proteins of interest; RTK, receptor tyrosine kinases; OSCs, ovarian somatic cells; BV, biliverdin; MPs, multimeric proteins; LDB, light-induced dimerization binder; FRAP, fluorescence recovery after photobleaching

REFERENCES

- (1) Rockwell, N. C.; Lagarias, J. C. A Brief History of Phytochromes. *ChemPhysChem* **2010**, *11*, 1172–1180.
- (2) Burgie, E. S.; Vierstra, R. D. Phytochromes: An Atomic Perspective on Photoactivation and Signaling. *Plant Cell* **2014**, *26*, 4568–4583.
- (3) Tan, P.; He, L.; Huang, Y.; Zhou, Y. Optophysiology: Illuminating cell physiology with optogenetics. *Physiol. Rev.* **2022**, *102*, 1263–1325.
- (4) Kawano, F.; Suzuki, H.; Furuya, A.; Sato, M. Engineered pairs of distinct photoswitches for optogenetic control of cellular proteins. *Nat. Commun.* **2015**, *6*, 6256.
- (5) Uda, Y.; Goto, Y.; Oda, S.; Kohchi, T.; Matsuda, M.; Aoki, K. Efficient synthesis of phycocyanobilin in mammalian cells for optogenetic control of cell signaling. *Proc. Natl. Acad. Sci. U.S.A.* **2017**, *114*, 11962–11967.
- (6) Kennedy, M. J.; Hughes, R. M.; Peteya, L. A.; Schwartz, J. W.; Ehlers, M. D.; Tucker, C. L. Rapid blue-light-mediated induction of protein interactions in living cells. *Nat. Methods* **2010**, *7*, 973–975.
- (7) Guntas, G.; Hallett, R. A.; Zimmerman, S. P.; Williams, T.; Yumerefendi, H.; Bear, J. E.; Kuhlman, B. Engineering an improved light-induced dimer (iLID) for controlling the localization and activity of signaling proteins. *Proc. Natl. Acad. Sci. U.S.A.* **2015**, *112*, 112–117.
- (8) Kögler, A. C.; Kherdjemil, Y.; Bender, K.; Rabinowitz, A.; Marco-Ferreres, R.; Furlong, E. E. M. Extremely rapid and reversible optogenetic perturbation of nuclear proteins in living embryos. *Dev. Cell* **2021**, *56*, 2348–2363.
- (9) Glantz, S. T.; Carpenter, E. J.; Melkonian, M.; Gardner, K. H.; Boyden, E. S.; Wong, G. K.; Chow, B. Y. Functional and topological diversity of LOV domain photoreceptors. *Proc. Natl. Acad. Sci. U.S.A.* **2016**, *113*, E1442–E1451.
- (10) Aoki, K.; Kumagai, Y.; Sakurai, A.; Komatsu, N.; Fujita, Y.; Shionyu, C.; Matsuda, M. Stochastic ERK Activation Induced by Noise and Cell-to-Cell Propagation Regulates Cell Density-Dependent Proliferation. *Mol. Cell* **2013**, *52*, 529–540.
- (11) Nihongaki, Y.; Yamamoto, S.; Kawano, F.; Suzuki, H.; Sato, M. CRISPR-Cas9-based Photoactivatable Transcription System. *Chem. Biol.* **2015**, 22, 169–174.
- (12) Nihongaki, Y.; Furuhata, Y.; Otabe, T.; Hasegawa, S.; Yoshimoto, K.; Sato, M. CRISPR—Cas9-based photoactivatable transcription systems to induce neuronal differentiation. *Nat. Methods* **2017**, *14*, 963—966.
- (13) Nihongaki, Y.; Kawano, F.; Nakajima, T.; Sato, M. Photoactivatable CRISPR-Cas9 for optogenetic genome editing. *Nat. Biotechnol.* **2015**, 33, 755–760.

- (14) Nihongaki, Y.; Otabe, T.; Ueda, Y.; Sato, M. A split CRISPR—Cpf1 platform for inducible genome editing and gene activation. *Nat. Chem. Biol.* **2019**, *15*, 882—888.
- (15) Kawano, F.; Okazaki, R.; Yazawa, M.; Sato, M. A photo-activatable Cre-loxP recombination system for optogenetic genome engineering. *Nat. Chem. Biol.* **2016**, *12*, 1059–1064.
- (16) Jung, H.; Kim, S.-W.; Kim, M.; Hong, J.; Yu, D.; Kim, J. H.; Lee, Y.; Kim, S.; Woo, D.; Shin, H.-S.; Park, B. O.; Heo, W. D. Noninvasive optical activation of Flp recombinase for genetic manipulation in deep mouse brain regions. *Nat. Commun.* **2019**, *10*, 314.
- (17) Lee, D.; Creed, M.; Jung, K.; Stefanelli, T.; Wendler, D. J.; Oh, W. C.; Mignocchi, N. L.; Lüscher, C.; Kwon, H.-B. Temporally precise labeling and control of neuromodulatory circuits in the mammalian brain. *Nat. Methods* **2017**, *14*, 495–503.
- (18) Pu, J.; Zinkus-Boltz, J.; Dickinson, B. C. Evolution of a split RNA polymerase as a versatile biosensor platform. *Nat. Chem. Biol.* **2017**, *13*, 432–438.
- (19) Yu, D.; Lee, H.; Hong, J.; Jung, H.; Jo, Y.; Oh, B.-H.; Park, B. O.; Heo, W. D. Optogenetic activation of intracellular antibodies for direct modulation of endogenous proteins. *Nat. Methods* **2019**, *16*, 1095–1100.
- (20) Liu, Q.; Sinnen, B. L.; Boxer, E. E.; Schneider, M. W.; Grybko, M. J.; Buchta, W. C.; Gibson, E. S.; Wysoczynski, C. L.; Ford, C. P.; Gottschalk, A.; Aoto, J.; Tucker, C. L.; Kennedy, M. J. A Photoactivatable Botulinum Neurotoxin for Inducible Control of Neurotransmission. *Neuron* **2019**, *101*, 863–875.
- (21) Lee, S.; Park, H.; Kyung, T.; Kim, N. Y.; Kim, S.; Kim, J.; Heo, W. D. Reversible protein inactivation by optogenetic trapping in cells. *Nat. Methods* **2014**, *11*, 633–636.
- (22) Doupé, D. P.; Perrimon, N. Visualizing and Manipulating Temporal Signaling Dynamics with Fluorescence-Based Tools. *Sci. Signal.* **2014**, *7*, re1.
- (23) Turgeon, B.; Meloche, S. Interpreting Neonatal Lethal Phenotypes in Mouse Mutants: Insights Into Gene Function and Human Diseases. *Physiol. Rev.* **2009**, *89*, 1–26.
- (24) Wargent, J. J.; Gegas, V. C.; Jenkins, G. I.; Doonan, J. H.; Paul, N. D. UVR8 in Arabidopsis thaliana regulates multiple aspects of cellular differentiation during leaf development in response to ultraviolet B radiation. *New Phytol.* **2009**, *183*, 315–326.
- (25) Chen, D.; Gibson, E. S.; Kennedy, M. J. A light-triggered protein secretion system. *J. Cell Biol.* **2013**, 201, 631–640.
- (26) Osswald, M.; Santos, A. F.; Morais-de-Sá, E. Light-Induced Protein Clustering for Optogenetic Interference and Protein Interaction Analysis in Drosophila S2 Cells. *Biomolecules* **2019**, *9*, 61.
- (27) Qin, X.; Park, B. O.; Liu, J.; Chen, B.; Choesmel-Cadamuro, V.; Belguise, K.; Heo, W. D.; Wang, X. Cell-matrix adhesion and cell-cell adhesion differentially control basal myosin oscillation and Drosophila egg chamber elongation. *Nat. Commun.* **2017**, *8*, 14708.
- (28) Lu, X.; Wen, Y.; Zhang, S.; Zhang, W.; Chen, Y.; Shen, Y.; Lemieux, M. J.; Campbell, R. E. Photocleavable proteins that undergo fast and efficient dissociation. *Chem. Sci.* **2021**, *12*, 9658–9672.
- (29) Kainrath, S.; Stadler, M.; Reichhart, E.; Distel, M.; Janovjak, H. Green-Light-Induced Inactivation of Receptor Signaling Using Cobalamin-Binding Domains. *Angew. Chem., Int. Ed. Engl.* **2017**, *56*, 4608–4611.
- (30) Lehtinen, K.; Nokia, M. S.; Takala, H. Red Light Optogenetics in Neuroscience. *Front. Cell. Neurosci.* **2022**, *15*, 778900.
- (31) Tang, K.; Beyer, H. M.; Zurbriggen, M. D.; Gärtner, W. The Red Edge: Bilin-Binding Photoreceptors as Optogenetic Tools and Fluorescence Reporters. *Chem. Rev.* **2021**, *121*, 14906–14956.
- (32) Kaberniuk, A. A.; Shemetov, A. A.; Verkhusha, V. V. A bacterial phytochrome-based optogenetic system controllable with near-infrared light. *Nat. Methods* **2016**, *13*, 591–597.
- (33) Zhou, Y.; Kong, D.; Wang, X.; Yu, G.; Wu, X.; Guan, N.; Weber, W.; Ye, H. A small and highly sensitive red/far-red optogenetic switch for applications in mammals. *Nat. Biotechnol.* **2022**, *40*, 262–272.

- (34) Bellini, D.; Papiz, M. Structure of a Bacteriophytochrome and Light-Stimulated Protomer Swapping with a Gene Repressor. *Structure* **2012**, *20*, 1436–1446.
- (35) Levskaya, A.; Weiner, O. D.; Lim, W. A.; Voigt, C. A. Spatiotemporal control of cell signalling using a light-switchable protein interaction. *Nature* **2009**, *461*, 997–1001.
- (36) Beyer, H. M.; Juillot, S.; Herbst, K.; Samodelov, S. L.; Müller, K.; Schamel, W. W.; Römer, W.; Schäfer, E.; Nagy, F.; Strähle, U.; Weber, W.; Zurbriggen, M. D. Red Light-Regulated Reversible Nuclear Localization of Proteins in Mammalian Cells and Zebrafish. ACS Synth. Biol. 2015, 4, 951–958.
- (37) Reichhart, E.; Ingles-Prieto, A.; Tichy, A. M.; McKenzie, C.; Janovjak, H. A Phytochrome Sensory Domain Permits Receptor Activation by Red Light. *Angew. Chem., Int. Ed. Engl.* **2016**, *55*, 6339–6342.
- (38) Redchuk, T. A.; Omelina, E. S.; Chernov, K. G.; Verkhusha, V. V. Near-infrared optogenetic pair for protein regulation and spectral multiplexing. *Nat. Chem. Biol.* **2017**, *13*, 633–639.
- (39) Bhoo, S.-H.; Davis, S. J.; Walker, J.; Karniol, B.; Vierstra, R. D. Bacteriophytochromes are photochromic histidine kinases using a biliverdin chromophore. *Nature* **2001**, *414*, 776–779.
- (40) Kuwasaki, Y.; Suzuki, K.; Yu, G.; Yamamoto, S.; Otabe, T.; Kakihara, Y.; Nishiwaki, M.; Miyake, K.; Fushimi, K.; Bekdash, R.; Shimizu, Y.; Narikawa, R.; Nakajima, T.; Yazawa, M.; Sato, M. A red light—responsive photoswitch for deep tissue optogenetics. *Nat. Biotechnol.* **2022**, *40*, 1672–1679.
- (41) Huang, Z.; Li, Z.; Zhang, X.; Kang, S.; Dong, R.; Sun, L.; Fu, X.; Vaisar, D.; Watanabe, K.; Gu, L. Creating Red Light-Switchable Protein Dimerization Systems as Genetically Encoded Actuators with High Specificity. ACS Synth. Biol. 2020, 9, 3322–3333.
- (42) Davis, S. J.; Vener, A. V.; Vierstra, R. D. Bacteriophytochromes: Phytochrome-Like Photoreceptors from Nonphotosynthetic Eubacteria. *Science* **1999**, *286*, 2517–2520.
- (43) Zhou, S.; Yamada, R.; Sakamoto, K.; Sakamoto, K. Low energy multiple blue light-emitting diode light Irradiation promotes melanin synthesis and induces DNA damage in B16F10 melanoma cells. *PLoS One* **2023**, *18*, No. e0281062.
- (44) Chamayou-Robert, C.; DiGiorgio, C.; Brack, O.; Doucet, O. Blue light induces DNA damage in normal human skin keratinocytes. *Photodermatol. Photoimmunol. Photomed.* **2022**, *38*, 69–75.
- (45) Ruggiero, E.; Alonso-de Castro, S.; Habtemariam, A.; Salassa, L. Upconverting nanoparticles for the near infrared photoactivation of transition metal complexes: new opportunities and challenges in medicinal inorganic photochemistry. *Dalton Trans.* **2016**, *45*, 13012—13020
- (46) Takala, H.; Bjorling, A.; Berntsson, O.; Lehtivuori, H.; Niebling, S.; Hoernke, M.; Kosheleva, I.; Henning, R.; Menzel, A.; Ihalainen, J. A.; Westenhoff, S. Signal amplification and transduction in phytochrome photosensors. *Nature* **2014**, *509*, 245–248.
- (47) Wagner, J. R.; Zhang, J.; von Stetten, D.; Gunther, M.; Murgida, D. H.; Mroginski, M. A.; Walker, J. M.; Forest, K. T.; Hildebrandt, P.; Vierstra, R. D. Mutational analysis of Deinococcus radiodurans bacteriophytochrome reveals key amino acids necessary for the photochromicity and proton exchange cycle of phytochromes. *J. Biol. Chem.* **2008**, 283, 12212–12226.
- (48) Ryan, M. D.; King, A. M. Q.; Thomas, G. P. Cleavage of foot-and-mouth disease virus polyprotein is mediated by residues located within a 19 amino acid sequence. *J. Gen. Virol.* **1991**, *72*, 2727–2732.
- (49) Liu, Z.; Chen, O.; Wall, J. B. J.; Zheng, M.; Zhou, Y.; Wang, L.; Ruth Vaseghi, H.; Qian, L.; Liu, J. Systematic comparison of 2A peptides for cloning multi-genes in a polycistronic vector. *Sci. Rep.* **2017**, *7*, 2193.
- (50) Leopold, A. V.; Chernov, K. G.; Shemetov, A. A.; Verkhusha, V. V. Neurotrophin receptor tyrosine kinases regulated with near-infrared light. *Nat. Commun.* **2019**. *10*. 1129.
- (51) Chernov, K.; Redchuk, T.; Omelina, E.; Verkhusha, V. V. Near-Infrared Fluorescent Proteins, Biosensors, and Optogenetic Tools Engineered from Phytochromes. *Chem. Rev.* **2017**, *117*, 6423–6446.

- (52) Wang, Z.; Zhang, G.; Zhang, H. Protocol for analyzing protein liquid—liquid phase separation. *Biophys. Rep.* **2019**, *5*, 1–9.
- (53) Li, P.; Banjade, S.; Cheng, H. C.; Kim, S.; Chen, B.; Guo, L.; Llaguno, M.; Hollingsworth, J. V.; King, D. S.; Banani, S. F.; Russo, P. S.; Jiang, Q. X.; Nixon, B. T.; Rosen, M. K. Phase transitions in the assembly of multivalent signalling proteins. *Nature* **2012**, *483*, 336–340.
- (54) Fongsuwan, C.; Tipparach, U. A study of the inverse square law using LCD display projectors. J. Phys.: Conf. Ser. 2021, 1719, 012093.
- (55) Al-Juboori, S. I.; Dondzillo, A.; Stubblefield, E. A.; Felsen, G.; Lei, T. C.; Klug, A. Light scattering properties vary across different regions of the adult mouse brain. *PLoS One* **2013**, *8*, No. e67626.
- (56) Sueoka, K.; Chikama, T.; Shinji, K.; Kiuchi, Y. Effectiveness of laser pulsed irradiation for antimicrobial photodynamic therapy. *Lasers Med. Sci.* **2024**, *39*, 151.
- (57) Zhao, E. M.; Suek, N.; Wilson, M. Z.; Dine, E.; Pannucci, N. L.; Gitai, Z.; Avalos, J. L.; Toettcher, J. E. Light-based control of metabolic flux through assembly of synthetic organelles. *Nat. Chem. Biol.* **2019**, *15*, 589–597.
- (58) Tan, P.; He, L.; Huang, Y.; Zhou, Y. Optophysiology: Illuminating cell physiology with optogenetics. *Physiol Rev.* **2022**, 102, 1263–1325.
- (59) Schneider, N.; Wieland, F. G.; Kong, D.; Fischer, A. A. M.; Horner, M.; Timmer, J.; Ye, H.; Weber, W. Liquid-liquid phase separation of light-inducible transcription factors increases transcription activation in mammalian cells and mice. *Sci. Adv.* **2021**, *7*, No. eabd 3568.
- (60) Shin, Y.; Berry, J.; Pannucci, N.; Haataja, M. P.; Toettcher, J. E.; Brangwynne, C. P. Spatiotemporal Control of Intracellular Phase Transitions Using Light-Activated optoDroplets. *Cell* **2017**, *168*, 159–171.e14.
- (61) Hernandez-Candia, C. N.; Brady, B. R.; Harrison, E.; Tucker, C. L. A platform to induce and mature biomolecular condensates using chemicals and light. *Nat. Chem. Biol.* **2024**, *20*, 452–462.
- (62) Vassilev, L. T. Cell cycle synchronization at the G2/M phase border by reversible inhibition of CDK1. *Cell Cycle* **2006**, *5*, 2555–2556
- (63) Okumura, D.; Hagino, M.; Yamagishi, A.; Kaibori, Y.; Munira, S.; Saito, Y.; Nakayama, Y. Inhibitors of the VEGF Receptor Suppress HeLa S3 Cell Proliferation via Misalignment of Chromosomes and Rotation of the Mitotic Spindle, Causing a Delay in M-Phase Progression. *Int. J. Mol. Sci.* 2018, 19, 4014.
- (64) Niopek, D.; Wehler, P.; Roensch, J.; Eils, R.; Di Ventura, B. Optogenetic control of nuclear protein export. *Nat. Commun.* **2016**, *7*, 10624.
- (65) Chen, X.; Zaro, J. L.; Shen, W. C. Fusion protein linkers: property, design and functionality. *Adv. Drug Deliv. Rev.* **2013**, *65*, 1357–1369.
- (66) Yang, G. G.; Xu, X. Y.; Ding, Y.; Cui, Q. Q.; Wang, Z.; Zhang, Q. Y.; Shi, S. H.; Lv, Z. Y.; Wang, X. Y.; Zhang, J. H.; Zhang, R. G.; Xu, C. S. Linker length affects expression and bioactivity of the onconase fusion protein in Pichia pastoris. *Genet. Mol. Res.* **2015**, *14*, 19360–19370.
- (67) Zimmer, A. M.; Pan, Y. K.; Chandrapalan, T.; Kwong, R. W. M.; Perry, S. F. Loss-of-function approaches in comparative physiology: is there a future for knockdown experiments in the era of genome editing? *J. Exp. Biol.* **2019**, 222, jeb175737.
- (68) Takala, H.; Lehtivuori, H.; Hammarén, H.; Hytönen, V. P.; Ihalainen, J. A. Connection between Absorption Properties and Conformational Changes in Deinococcus radiodurans Phytochrome. *Biochemistry* **2014**, *53*, 7076–7085.
- (69) Van Audenhove, I.; Gettemans, J. Nanobodies as Versatile Tools to Understand, Diagnose, Visualize and Treat Cancer. *EBioMedicine* **2016**, *8*, 40–48.
- (70) Alexander, E.; Leong, K. W. Discovery of nanobodies: a comprehensive review of their applications and potential over the past five years. *J. Nanobiotechnol.* **2024**, 22, 661.

- (71) Haruki, H.; Nishikawa, J.; Laemmli, U. K. The Anchor-Away Technique: Rapid, Conditional Establishment of Yeast Mutant Phenotypes. *Mol. Cell* **2008**, *31*, 925–932.
- (72) Port, F.; Chen, H.-M.; Lee, T.; Bullock, S. L. Optimized CRISPR/Cas tools for efficient germline and somatic genome engineering in Drosophila. *Proc. Natl. Acad. Sci. U.S.A.* **2014**, *111*, E2967–E2976.
- (73) Ran, F. A.; Hsu, P. D.; Wright, J.; Agarwala, V.; Scott, D. A.; Zhang, F. Genome engineering using the CRISPR-Cas9 system. *Nat. Protoc.* **2013**, *8*, 2281–2308.
- (74) Nakayama, Y.; Saito, Y.; Soeda, S.; Iwamoto, E.; Ogawa, S.; Yamagishi, N.; Kuga, T.; Yamaguchi, N. Genistein Induces Cytokinesis Failure Through RhoA Delocalization and Anaphase Chromosome Bridging. *J. Cell. Biochem.* **2014**, *115*, 763–771.
- (75) Nakayama, Y.; Matsui, Y.; Takeda, Y.; Okamoto, M.; Abe, K.; Fukumoto, Y.; Yamaguchi, N. c-Src but Not Fyn Promotes Proper Spindle Orientation in Early Prometaphase. J. Biol. Chem. 2012, 287, 24905–24915.